the region grouping procedure starts from the initial block $b_0$, selects mergeable blocks from the 1st neighbors, the 2nd neighbors, $\cdots$, etc. Suppose we examine the neighboring blocks according to the order of NBL list, and obtain a region $R_i$ where

$$\max(R_i) = \max(b_1^k);$$

now let $R_i'$ be the grouped region just before examining the $k$th neighbors; then, the image $I(x, y)$ can be a function such that

$$\max(b_1^k) - \min(b_{n_k}^k) > 2e \ (\text{so } b_{n_k}^k \bar{\in} R_i)$$

and

$$\max(R_i') - \min(b_{n_k}^k) < 2e$$

are both true, here $e$ is the tolerance value. Thus, if we start examining the $k$th neighbors in the order $b_{n_k}^k, b_{n_k-1}^k, \cdots, b_2^k, b_1^k$ to form another region result, $\hat{R}_i$, then

$$b_{n_k}^k \in \hat{R}_i,\ b_1^k \bar{\in} \hat{R}_i;$$

$$b_1^k \in R_i,\ b_{n_k}^k \bar{\in} R_i;$$

hence

$$\hat{R}_i \neq R_i. \qquad \square$$

## Appendix B

*Proof:* Let us express the neighboring block list NBL as

$$\text{NBL} = \left\{(b_0)\ (b_1^1, b_2^1, \cdots, b_{k_1}^1) \cdot (b_{k_1+1}^2, b_{k_1+2}^2, \cdots, b_{k_1+k_2}^2) \cdots \right\},$$

where $b_0$ is the initial block, $\{b_k^i\}$ are $i$th neighbors of $b_0$, and $k$ is numbered according to the block examining sequence of the grouping algorithm.

Since $b_f$ is in NBL, suppose $b_f = b_m^i$; then

$$b_n^j \in T_2, \qquad \text{for any } j \leq i,\ n < m;$$

thus, starting from $b_0$, both grouping on tile $T_2$ and on the whole image $I$, are just examining blocks in NBL from $b_1^1$ to $b_{m-1}^i$ (or $b_{m-1}^{i-1}$) and merge the block if it satisfies the same uniformity criteria. Hence, the grouped results just before examining the block $b_f = b_m^i$, are exactly the same for both cases. $\square$

## Acknowledgment

We gratefully appreciate the help of J. G. Hauk and Y. T. Liow who provided us with their software tools and the standard split-and-merge segmentation program.

## References

[1] J. D. Browning and S. L. Tanimoto, "Segmentation of pictures into regions with a tile-by-tile method," *Pattern Recogn.*, vol. 14, no. 1, pp. 1-10, 1982.
[2] A. Rosenfeld and A. Y. Wu, "Parallel computer for region-level image processing," *Pattern Recogn.*, vol. 15, no. 1, pp. 41-50, 1982.
[3] J. Serra, *Image Analysis and Mathematical Morphology*. London: Academic, 1982.
[4] T. Pavlidis, "An asynchronous thinning algorithm," *Comput. Graphics, Image Processing*, vol. 20, pp. 133-157, 1982.
[5] S. L. Horowitz and T. Pavlidis, "Picture segmentation by a tree traversal algorithm," *J. ACM*, vol. 23, pp. 368-388, 1976.
[6] T. Pavlidis, *Structural Pattern Recognition*. New York: Springer-Verlag, 1977.
[7] R. M. Haralick, "Survey: Image segmentation techniques," *Comput. Vision, Graphics, Image Processing*, vol. 29, no. 1, 1985.
[8] P. C. Chen and T. Pavlidis, "Segmentation by texture using a co-occurrence matrix and a split-and-merge algorithm," *Comput. Graphics, Image Processing*, vol. 10, pp. 172-182, 1979.
[9] M. F. Doherty, M. T. Noga, and C. M. Bjorklund, "Use of compound predicates in split-and-merge segmentation," in *Proc. CVPR 85*, San Francisco, CA, pp. 659-661.
[10] R. H. Laprade and M. F. Doherty, "Split-and-merge segmentation using an F test criterion," *Proc. SPIE—Int. Soc. Opt. Eng.*, vol. 758, pp. 74-79, 1987.
[11] P. Bouthemy and J. S. Rivero, "A hierarchical likelihood approach for region segmentation according to motion-based criteria," in *Proc. 1st Int. Conf. Computer Vision*, 1987, pp. 463-467.
[12] R. Gershon, A. D. Jepson, and J. K. Tsotsos, "Highlight identification using chromatic information," in *Proc. 1st Int. Conf. Computer Vision*, 1987, pp. 161-170.

# Modified Matched Filter for Cloud Clutter Suppression

WILLIAM A. C. SCHMIDT

***Abstract*—Advanced surveillance sensor systems for point target detection are sometimes limited more by background clutter than by sensor noise. A significant premium is placed on the ability to develop clutter suppression processes that approach clear sky performance. In most actual infrared systems cloud clutter has been noted to have a nonwhite clutter spectrum. This prompted the consideration of alternatives to the classical matched filter (MF). A development known as the least-mean-square (LMS) filter addresses the clutter spectrum issue.**

**Another difficulty has surfaced and is the subject of this correspondence: the output of the MF and the LMS processes are dependent on the scene energy and are marginally dependent on the filter signal shape. An approach is presented, referred to as the modified matched filter (MMF). The MMF is a product of the LMS filter and a nonlinear operator, called the inverse Euclidean distance. The nonlinear operator modifies the LMS filter to improve its sensitivity to signal shape. A comparison is presented to indicate the relative merit for including shape detection in the LMS clutter suppression process.**

**Infrared cloud scenes from the background measurements and analysis program (BMAP) were used to demonstrate the relative clutter suppression performance for both the LMS and the MMF processes.**

**A performance metric is developed to measure cloud clutter suppression quantitatively. The results using the BMAP infrared cloud scenes indicate that the MMF approach suppresses cloud clutter while improving point target observability. The metric results indicate that on average, the MMF approach suppresses cloud clutter and improves point target detection by a factor of 4.4 over the conventional approach.**

***Index Terms*—Cloud clutter suppression, Euclidean distance, infrared image processing, matched filter, nonstationary clutter statistics, signal shape matching, template matching, unresolved target detection.**

## I. Background

Considerable attention has been given to the problem of extracting information from sensor video data to determine the presence or absence of target type signals. The extraction or detection of a deterministic signal in white, Gaussian noise has been studied by a number of authors (e.g., North [1] and Van Vleck and Middleton [2]). These authors found that optimum response (on a signal-to-

Manuscript received July 12, 1988; revised December 28, 1989. Recommended for acceptance by J. L. Mundy.

The author is with the Naval Air Development Center, Department of Mission Avionics Technology, Warminster, PA 18974.

IEEE Log Number 9034829.

noise ratio (SNR) basis) occurs with the cross-correlation of the input data and the desired signal waveform. The signal waveform is an amplitude function in a given coordinate system (called signal shape). The cross-correlation process is often referred to as a matched filter (MF). The MF process has been applied for clutter suppression in infrared (IR) scenes. Assume a two-dimensional IR scene with scene intensity $D(I, J)$ located in the $I, J$ coordinate system. Assume a two-dimensional filter kernel with an amplitude $F(I, J)$. The discrete MF in two dimensions is represented by:

$$\mathrm{MF}(M, N) = \sum \sum D(I - M, J - N)F(I, J) \qquad (1)$$

where $I = 1, 2, 3, \cdots, n$ and $J = 1, 2, 3, \cdots, m$ and $M, N$ are locations in the $I, J$ coordinate system.

In most actual infrared sensor systems, cloud clutter has been noted to have a nonwhite clutter spectrum. This prompted the consideration of alternatives to the classical matched filter approach for suppressing cloud clutter and to improve target type signal detection. A development known as the least-mean-square filter (LMS) (Longmire *et al.* [3]) addresses the clutter spectrum issue. The LMS filter (also known as the zero-mean matched filter) is represented by:

$$\begin{aligned}\mathrm{LMS}(M, N) &= \sum \sum D(I - M, J - N)\left[F(I, J) - F_0\right] \\ &= \sum \sum D(I - M, J - N)F'(I, J) \qquad (2)\end{aligned}$$

where $F'(I, J)$, is LMS filter shape such that $\Sigma\Sigma F'(I, J) = 0.0$.

The LMS approach was designed to suppress cloud clutter assuming the clutter statistics to be globally stationary processes, with a one over frequency squared ($1/f^2$) power spectrum. From this perspective the LMS processing represents an optimal approach. However, the LMS performance degrades against severe cloud clutter backgrounds. Since the early 1980's, LMS spatial filters were used to suppress background clutter. Today the LMS process serves as a baseline for comparing clutter suppression improvements.

Another difficulty has surfaced and is the subject of this paper: the output of both the MF and the LMS are dependent on scene energy and is marginally dependent on signal shape. This effect has been reported by others as, "The maximum SNR for the MF is independent of the signal shape and depends only on the ratio of signal energy to noise spectral density" [4]. The question arises: Can anything be done to improve the clutter suppression by modifying the MF with a signal shape related operator?

We are interested in detecting distant objects. They are often called point targets because they appear as impulses to the imaging system. The imaging system impulse response is often called the point spread function (PSF) for that system. Distant objects transfer to the image with a radiant intensity amplitude that is proportional to the PSF. Point spread functions (typically 3–10 pixels on a side) then represent the signal shape for a point target. The PSF is used to form the MF kernel $F(I, J)$ when a point target is suspected to be in the image. We will attempt to improve the clutter suppression performance by modifying the MF with a signal shape related operator.

## II. Modified Matched Filter

It is interesting that another branch of technology, namely, image processing, uses a cross-correlation approach known as "template matching" [5] to determine the presence of an object within an image. Template matching is typically used for matching areas of the scene with a given area-type template. Some similarity measures or metrics for template matching have been suggested (such as the sum of the absolute differences, invariant moments, and the cross-correlation coefficient), to determine the presence of an object within an image. The point of interest is that both the MF approach and template matching approach use the cross-correlation type process to extract the desired information. It seems that the next logical step is to transform the template matching technology into a target shape detection technology.

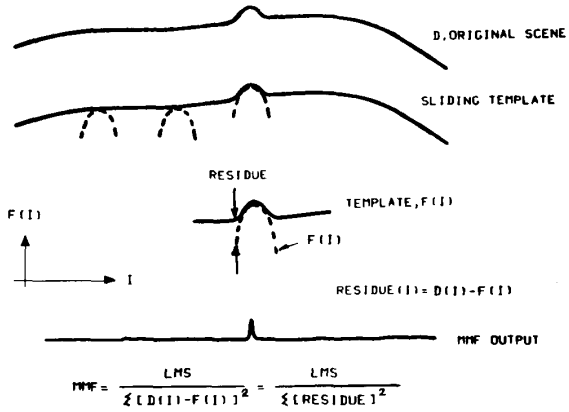


Fig. 1. Modified matched filter graphic representation.

From this point on, we consider only a one-dimensional filter kernel $F(I)$. This kernel is correlated across the image along one row at a time. A modifier is suggested that takes the difference between the filter $F(I)$ and the image amplitude $D(I - M)$ at the row coordinate $M$. We call this difference the residue. The smaller the residue the better the fit between the filter (or template) and the image. Fig. 1 graphically illustrates how a residue type operator could be used to improve the ubiquitous MF or the LMS filter.

The Euclidean distance (in one dimension) is square root of the sum of the squares of the residues. It is represented by:

$$E(M) = \sqrt{\sum \left[D(I - M) - F(I)\right]^2} \qquad (3)$$

where $D(I - M)$ is the input scene and $F(I)$ is the desired one-dimensional filter shape.

The filter is translated within the image position by $M$. An operator is proposed, that is related to the inverse Euclidean distance (IED). It serves as a multiplier to improve the shape sensitivity of the LMS filter. IED is represented by

$$\mathrm{IED} = \frac{1}{\sum \left[D(I - M) - F(I) - \left(D(n/2) - F(n/2)\right)\right]^2} \qquad (4)$$

where $n$ is number of elements in the filter ($n$ is odd). The central $D - F$ value is subtracted to offset the filter in the vertical direction and causes the filter to fit perfectly at the central pixel of the data window.

We form a product called the modified matched filter (MMF).

$$\mathrm{MMF} = (\mathrm{LMS})(\mathrm{IED}) \qquad (5)$$

$$\mathrm{MMF} = \frac{\sum D(I - M)\left(F(I) - F_0\right)}{\sum \left[D(I - M) - F(I) - \left(D(n/2) - F(n/2)\right)\right]^2} \qquad (6)$$

The MMF processor output for the signal-plus-noise case (see Appendix A) is

$$\mathrm{MMF}(S + N) = \frac{F(SK_0 + K_1)}{(S - F)^2K_3 + 2(S - F)K_4 + K_5}. \qquad (7)$$

The MMF processor output for noise only (See Appendix A) is:

$$\mathrm{MMF}(N) = \frac{FK_1}{F^2K_3 - 2FK_4 + K_5} \qquad (8)$$

where $K_i$ are constants for a given signal and noise case (see Appendix A). Also, $S$ is the peak signal strength and $F$ is the peak filter value.

## III. IR Clutter Suppression

Consider the problem of suppressing the clutter in order to detect a $(1 \times n)$ point target signal (produced by a distant object). In this case, we process a two-dimensional image one row at a time. We wish to formulate a metric for comparing the clutter suppression performance of both the LMS and the MMF processes using the same signal and noise basis. The MMF approach operates on the image pixels in a nonlinear fashion. Therefore we will not use the classic SNR metric. Instead, we consider the signal detection performance in terms of signal plus noise. We define a clutter suppression metric "performance ratio" (PR) as follows:

$$\mathrm{PR(Process)} = \frac{\text{Process Output (Signal + Noise)}}{\text{Process Output (Noise)}}. \quad (9)$$

In general, higher PR values indicate better clutter suppression by a given process.

The performance ratio for the LMS process is (see Appendix B)

$$\mathrm{PR(LMS)} = 1 + SK_0/K_1. \quad (10)$$

The PR for the MMF process is (see Appendix B)

$$\mathrm{PR(MMF)} = \frac{K_2(SK_0 + K_1)}{K_1\left[(S-F)^2K_3 + 2(S-F)K_4 + K_5\right]}. \quad (11)$$

Notice the PR(LMS) is a linear function of the peak signal strength $S$. On the other hand, the PR(MMF) contains the inverse quadratic function in $(S - F)$. This functional behavior indicates that the MMF is sensitive to the selection of the peak filter value $F$. Ideally, we would select $F = S$ to maximize the PR(MMF). The expected $S$ values are on the order of 1–100 counts. Count is a unit of radiant intensity measure. Normally, we do not have the information for the precise value of $S$ for a particular scene *a priori*. Therefore, it is important to indicate the relative merit of the MMF process even without the knowledge of the precise value of $S$. The relative PR values under various clutter conditions in the following example will provide some insight into this question.

### A. Clutter Suppression Example

Assume an imaging system with an optical point spread function that can be represented by seven pixels ($n = 7$). Assume a Gaussian shaped PSF, (mean = 4, sigma = 1). Then the $\alpha(I)$ values are:

$$0.01,\ 0.14,\ 0.61,\ 1.0,\ 0.61,\ 0.14,\ 0.01.$$

Assume a noise function to represent cloud clutter as follows:

$$N(I) = N_0 + R + A * I, \quad I = 1, 2, 3, \cdots, n \ \text{(counts)} \quad (12)$$

where $N_0$ is constant, $N_0 = 100$ for clear sky and 1200 for clouds, $R$ is uniformly distributed random noise (counts), $A$ is the ramp rate (represents transition between clear sky and cloud regions) (counts/pixel).

Also let

$$\theta(I) = \mathrm{N(I)}/N(4). \quad (13)$$

Table I illustrates the PR values for the LMS and the MMF processes at $S = F$ for various simulated cloud conditions (using the signal and noise conditions prescribed above). The PR values in Table I are averages taken over 100 samples (using positive PR(LMS) values only). Notice, that PR(MMF) is sensitive to the magnitude of the ramp, because the MMF approach is sensitive to the signal shape. Steep ramps tend to distort the signal shape. However, the PR(MMF) values exceed the PR(LMS) values by a considerable factor, for all of the cases tested.

Additional PR values where compiled for $S$ not equal to $F$ cases. The results are illustrated in Figs. 2–4. The PR values for the PR(LMS) and PR(MMF) are plotted on a common signal strength $S$ abscissa axis. Notice, the quadratic nature for PR(MMF), with a peak values in the $S = F$ neighborhood. Figs. 2 and 3 illustrate the effect of different $F$ values at a low cloud transition ramp value ($A = 1$). Fig. 4 uses the same parameters as Fig. 3 except for a steeper ramp value ($A = 5$). These figures illustrate the $F$ dependence and the noise ramp dependence of the MMF process. The point of this simulated clutter suppression example is to illustrate that it is not necessary to prescribe the precise value of $F$ in order for the MMF process to show a significant improvement over the original LMS process. In fact, these examples indicate that the MMF is better than the LMS provided the selected $F$ value is within plus or minus 50% of the actual $S$ value. In the next section, we consider a more realistic demonstration of the relative value of the LMS and the MMF processes using actual flight recorded infrared imagery.

TABLE I
AVERAGE PERFORMANCE RATIO**

| PR(LMS) S=40 | MAX PR(MMF) S=F=40 | CONSTANT $N_0$ (Counts) | RAMP RATE A | REMARKS |
|---|---|---|---|---|
| 79 | 29446 | 200 | 0 | Clear Sky |
| 79 | 719 | 200 | 5 | Low Ramp Rate |
| 79 | 240 | 200 | 10 | Mid Value |
| 79 | 119 | 200 | 20 | Mid Value |
| 79 | 89 | 200 | 40 | High Value |
| 79 | 29446 | 1200 | 0 | Benign Cloud |

** Average using 100 samples using uniformly distributed Random number times 5
Same initial kernel for each trial

## IV. IR Clutter Suppression

IR cloud scenes from the background measurements and analysis program (BMAP) are used for algorithm evaluation purposes. The BMAP data set consists airborne collected cloud scenes using a dual-band radiometer with a field of view 2.2 degree in azimuth and 0.31 degree in elevation. The data set contains cloud and sky scenes from the Lake Erie area and the Gulf of Mexico area. The scenes used for this study are exclusively from the long wave IR band (8–12 microns). A BMAP cloud scene (15 × 346 pixels) known as the "cumulus cloud edge" was selected for this one sample demonstration. This scene is well suited for comparing the LMS and MMF clutter suppression algorithms because it contains many different cloud clutter regions. Two different test conditions were imposed: 1) original BMAP scene without point targets and 2) BMAP scene with five point targets ($S = 43$ counts) parametrically inserted into the original scene. These two conditions were necessary in order to calculate the respective PR values. Figs. 5 and 6 are "carpet plots" illustrating the clutter suppression test results. These figures consist of three different plots: the top plot represents the original BMAP scene, the middle plot represents the MMF output ($F = 56$), and the bottom plot represents the LMS output. The $F$ value was deliberately selected to be 53% different than the best $F = S$ value to illustrate the effectiveness of MMF despite this obvious mismatch. Notice that for the most part the MMF and LMS plots are similar, except at the point target locations. The MMF values at the point target locations are considerably larger than MMF values in the neighboring noise regions. These MMF prominences indicate regions where the signal shape matching is most effective. On the other hand, the LMS plot (baseline approach) does not have these target prominences. This indicates potential point target detection improvements offered by MMF clutter suppression. Table II presents the relative PR values for these target locations. The PR(MMF) values are higher on average than the PR(LMS) values by a factor of 4.4

Fig. 7 further illustrates the relative clutter suppression performance using a different BMAP scene with five targets at a lower signal strength ($S = 20$ counts). The $F$ value was the same as for

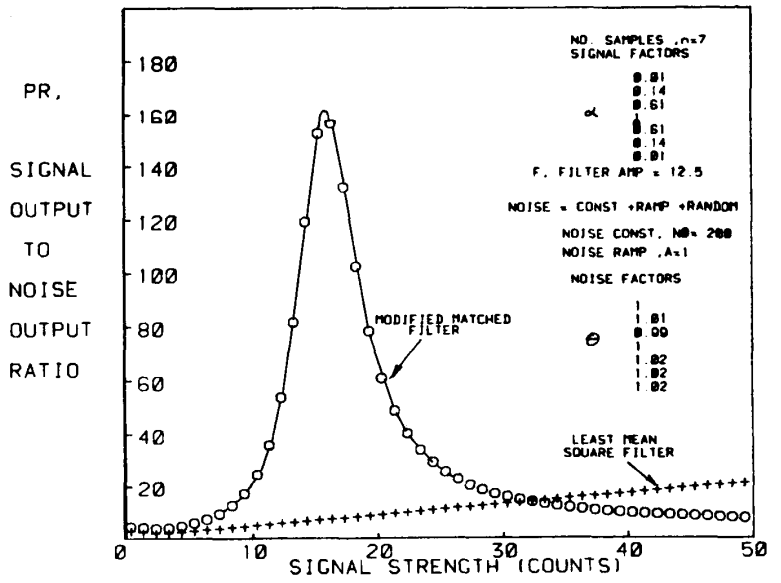


Fig. 2. Performance ratio ($F = 12.5$, $A = 1$).

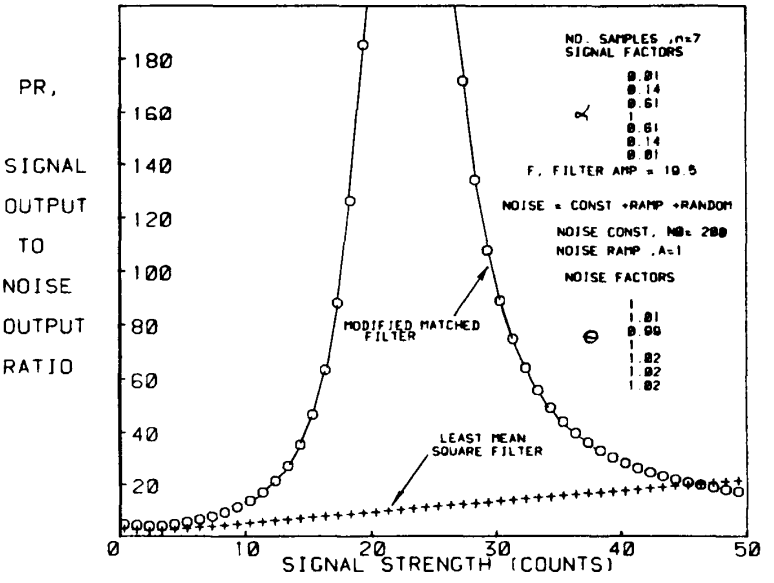


Fig. 3. Performance ratio ($F = 19.5$, $A = 1$).

the previous figures ($F = 56$). In this case, the $F$ and $S$ values differ by 180%. The MMF clutter suppression performance remains better than the original LMS process.

## V. Closing Remarks

These results illustrate that it is possible to achieve greater clutter suppression performance than provided by the conventional LMS filter. The key to this success appears to be the advantage offered by the signal shape detection factor given by the IED operator.

### A. MMF Sensitivity

The $F$ value sensitivity did not appear to be detrimental for the MMF clutter suppression performance in this data set. If the $F$ value selection does cause some difficulty with a different data set, then one possible solution is to apply multiple MMF processes in parallel (each at a different $F$ value). In this way the entire range of potential $S$ values can be processed.

### B. Computational Cost

Additional computation is required to implement the MMF process in place of the LMS process. In high level computer language this represents four additional lines of computer code over the existing LMS computer code. Continued investigation will determine the "cost-benefit" ratio of the required additional processing.

### C. Further Applications

The results presented here are for one dimensional filters only. The MMF approach could be extended to include two-dimensional filters. Of course, any improvement by a two-dimensional MMF

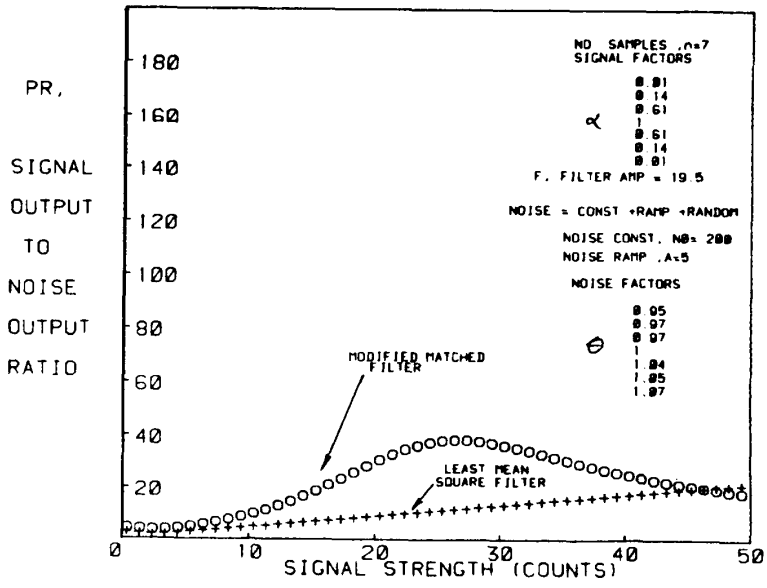


Fig. 4. Performance ratio ($F = 19.5$, $A = 5$).

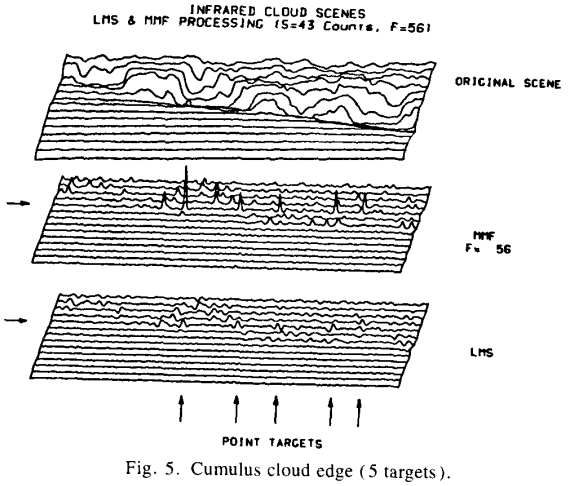


Fig. 5. Cumulus cloud edge (5 targets).

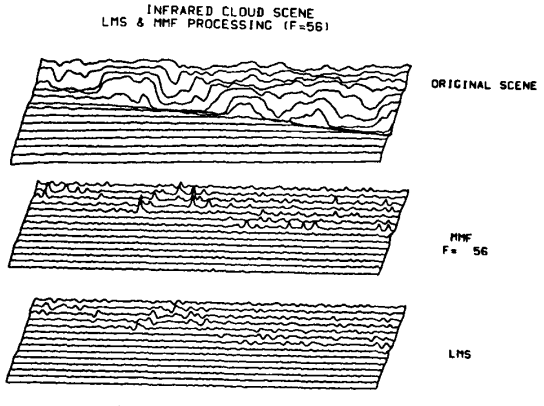


Fig. 6. Cumulus cloud edge (no targets).

TABLE II
PERFORMANCE RATIO (CUMULUS CLOUD EDGE)

| TGT CENTER (Pixel) | PR(MMF) | PR(LMS) | RATIO MMF / LMS |
|---|---|---|---|
| 124 | 105.8 | 16.1 | 6.6 |
| 174 | 36.8 | 9.8 | 3.7 |
| 210 | 28.4 | 5.7 | 4.9 |
| 261 | 32.8 | 7.1 | 4.6 |
| 285 | 8.1 | 3.3 | 2.4 |
| | | AVERAGE = | 4.4 |

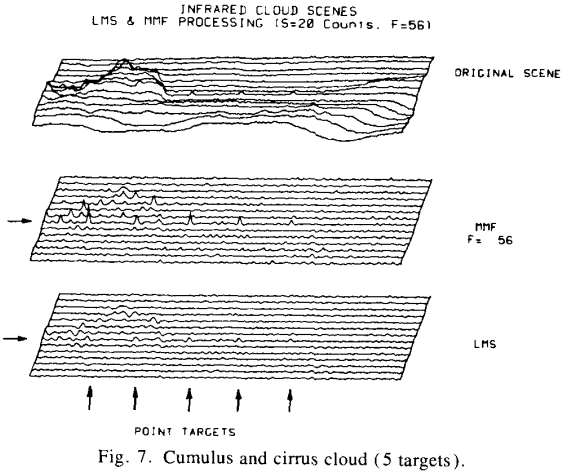


Fig. 7. Cumulus and cirrus cloud (5 targets).

filter must be large enough to warrant the additional computation load. The approach taken and the results achieved suggest that the MMF approach is applicable to other clutter suppression applications where the clutter statistics are nonstationary and the target signal has shape (i.e., not an impulse). Also, it is possible that the MMF approach may be extended to other conventional MF appli-

cations were signal shape rather than signal energy is the desired discriminate.

## Appendix A
## LMS and MMF Filter Output

Assume a symmetrical signal sequence can be represented by

$$S(I) = S\alpha(I), \quad I = 1, 2, 3, \cdots, n, \tag{A1}$$

where $n$ is odd,

$$0 \le \alpha(I) < 1$$

and

$$\alpha(1) = \alpha(n)$$
$$\alpha(2) = \alpha(n-1)$$
$$\alpha(3) = \alpha(n-2), \text{ etc.}$$

Also, $\alpha(n/2) = 1.0$ and $\alpha(1) < \alpha(2) < \alpha(3) < \cdots < \alpha(n/2)$. We represent a symmetrical filter function by

$$F(I) = F\alpha(I). \tag{A2}$$

Assume the noise sequence can be represented by

$$N(I) = N\theta(I), \tag{A3}$$

where $\theta(n/2) = 1$, and $N = N(n/2)$. Also $\theta(I)$ are noise factors at $I$.

A special case of the matched filter is the LMS (also called the suppressed-mean matched filter). In this case the filter function becomes

$$F'(I) = F\alpha(I) - F_0,$$

where

$$F_0 = \frac{F}{n}\sum \alpha(I). \tag{A4}$$

Assume noise is additive; then the LMS output for the signal-plus-noise case is

$$\mathrm{LMS}(S+N) = \sum\left[F\left(\alpha(I) - \frac{\sum \alpha(I)}{n}\right)\right]\left[S\alpha(I) + N\theta(I)\right]. \tag{A5}$$

The LMS output for the noise-only case is

$$\mathrm{LMS}(N) = \sum\left[F\left(\alpha(I) - \frac{\sum \alpha(I)}{n}\right)\right]N\theta(I). \tag{A6}$$

The values $N$, $\alpha(I)$, $\theta(I)$ are constant for any one given signal shape and any one given noise sequence.

The IED value for the signal-plus-noise case is

$$\mathrm{IED}(S+N) = \frac{1}{\sum\left[S\alpha(I) + N\theta(I) - F\alpha(I) - (S+N-F)\right]^2}. \tag{A7}$$

Notice the midvalue (at $I = n/2$) of $S + N - F$ is subtracted to offset the filter in the vertical direction and cause the filter to fit perfectly at the central pixel of the data window. Equation (A7) expands to

$$\mathrm{IED}(S+N) = \frac{1}{(S-F)^2\sum(\alpha(I)-1)^2 + 2N(S-F)\sum(\alpha(I)-1)(\theta(I)-1) + N^2\sum(\theta(I)-1)^2}. \tag{A8}$$

The IED value for the noise case is

$$\mathrm{IED}(N) = \frac{1}{\sum\left[N\theta(I) - F(\alpha(I)-1) - N\right]^2}. \tag{A9}$$

$$\mathrm{IED}(N) = \frac{1}{N^2\sum(\theta(I)-1)^2 - 2FN\sum(\alpha(I)-1)(\theta(I)-1) + F^2\sum(\alpha(I)-1)^2}. \tag{A10}$$

Let

$$K_0 = \sum\left(\alpha(I)^2 - \frac{\alpha(I)}{n}\sum\alpha(I)\right)$$
$$K_1 = N\sum\left(\theta(I)\alpha(I) - \frac{\theta(I)}{n}\sum\alpha(I)\right)$$
$$K_2 = \sum\left[N(\theta(I)-1) - F(\alpha(I)-1)\right]^2$$
$$K_3 = \sum(\alpha(I)-1)^2$$
$$K_4 = N\sum(\alpha(I)-1)(\theta(I)-1)$$
$$K_5 = N^2\sum(\theta(I)-1)^2.$$

The MMF processor output for the signal-plus-noise case is

$$\mathrm{MMF}(S+N) = \mathrm{LMS}(S+N)\mathrm{IED}(S+N).$$

In terms of the above constants it becomes

$$\mathrm{MMF}(S+N) = \frac{F(SK_0 + K_1)}{(S-F)^2K_3 + 2(S-F)K_4 + K_5}. \tag{A11}$$

The MMF processor output for the noise only case is

$$\mathrm{MMF}(N) = \frac{FK_1}{F^2K_3 - 2FK_4 + K_5}. \tag{A12}$$

## Appendix B
## LMS and MMF Performance Ratios

We define a clutter suppression metric, performance ratio PR:

$$\mathrm{PR}(\mathrm{Process}) = \frac{\text{Process Output (Signal + Noise)}}{\text{Process Output (Noise)}}. \tag{B1}$$

The performance ratio for the LMS process is

$$\mathrm{PR}(\mathrm{LMS}) = \frac{\mathrm{LMS}(\text{Signal + Noise})}{\mathrm{LMS}(\text{Noise})} \tag{B2}$$

where

$$\mathrm{LMS}(S+N) = \sum F\left[\left(\alpha(I) - \frac{\sum\alpha(I)}{n}\right)\right] \cdot \left[S\alpha(I) + N\theta(I)\right] \tag{B3}$$

and

$$\mathrm{LMS}(N) = \sum F\left[\alpha(I) - \frac{\sum \alpha(I)}{n}\right] N(I). \quad \text{(B4)}$$

Rewrite these equations in terms of the process constants $K_1$ (see Appendix A):

$$\mathrm{LMS}(S + N) = F(SK_0 + K_1) \quad \text{(B5)}$$

and

$$\mathrm{LMS}(N) = FK_1. \quad \text{(B6)}$$

Then the performance ratio for the LMS process is

$$\mathrm{PR}(\mathrm{LMS}) = 1 + SK_0/K_1 \quad \text{(B7)}$$

and the performance ratio for the MMF process is

$$\mathrm{PR}(\mathrm{MMF}) = \frac{\mathrm{MMF}(\mathrm{Signal} + \mathrm{Noise})}{\mathrm{MMF}(\mathrm{Noise})}. \quad \text{(B8)}$$

From (A11) and (A12) we have

$$\mathrm{MMF}(S + N) = \frac{F(SK_0 + K_1)}{(S - F)^2K_3 + 2(S - F)K_4 + K_5} \quad \text{(B9)}$$

$$\mathrm{MMF}(N) = \frac{FK_1}{F^2K_3 + 2FK_4 + K_5}. \quad \text{(B10)}$$

Then

$$\mathrm{PR}(\mathrm{MMF}) = \frac{K_2[SK_0 + K_1]}{K_1[(S - F)^2K_3 + 2(S - F)K_4 + K_5]}. \quad \text{(B11)}$$

## References


[1] D. O. North, "An analysis of the factors which determine signal/noise discrimination in pulsed carrier systems," RCA Labs., Princeton, NJ, Rep. PTR-6C, 1943.

[2] J. H. Van Vleck and D. A. Middleton, "Theoretical comparison of the visual, aural, and meter reception of pulsed signals in the presence of noise," *J. Appl. Phys.*, vol. 17, pp. 940–971, Nov. 1946.

[3] M. S. Longmire, A. F. Milton, and E. H. Takken, "Simulation of mid-infrared clutter rejection. 1. One-dimensional LMS spatial filter and adaptive threshold algorithms," *Appl. Opt.*, vol. 21, p. 3819, Nov. 1, 1982.

[4] H. Stark and F. B. Tuteur, *Modern Electrical Communications Theory and Systems*. Englewood Cliffs, NJ: Prentice-Hall, 1979, p. 488.

[5] R. O. Duda and P. E. Hart, *Pattern Classification and Scene Analysis*. New York: Wiley, 1973, pp. 276–284.


# Character Scaling by Contour Method

A. NAMANE AND M. A. SID-AHMED

***Abstract*—The advancement in digital image processing hardware has provided the printing industry with new facilities for capturing fonts. This has provided new grounds for character scaling which is an important issue in typesetting and graphical text.**

**An algorithm for digital character scaling by a contour method is developed and implemented. The algorithm is based on scaling the contour of the character through a transformation. Cubic splines are used to interpolate the discrete samples of the contour character. Final results are excellent, showing no "jaggies."**

**The algorithm is applied to Arabic fonts and compared to two other algorithms.**

***Index Terms*—Border following, interpolation, magnification, minification, template, thresholding.**

Manuscript received May 23, 1988; revised November 23, 1989. Recommended for acceptance by C. Y. Suen.

The authors are with the Department of Electrical Engineering, University of Windsor, Windsor, Ont. N9B 3P4, Canada.

IEEE Log Number 9034375.

## I. Introduction

Scaling in general is the process performed on the digital image input, which results in a digital image output of a different size, using magnification or minification.

A well known method for font scaling is that of replication [1]. This, however, results in pronounced jagged edges when the character is magnified.

The work done by Ulichney and Troxel [2], [3] utilized the telescoping template for scaling binary images of characters. The templates could be of any size, and the quality of the scaled font is dependent on the size of the template. The larger the size, the better the quality. Results for up to third order window scaling are presented in this correspondence. These results are reasonably good, except that for large enlargements there are some appearances of jaggies.

Casey, Friedman, and Wong [4] developed a scaling method which makes use of attributes associated with print character quality in order to suppress distortion and maintain essential features of the character. The smoothing step is carried out by a simple edge filter. The enlarged fonts exhibit some appearance of jaggies.

In the commercial world a number of page description languages are available [5]. Three languages have emerged as the leading standards: PostScript, $T_EX$, and InterPress. Of the three, PostScript seems to be taking a clear leadership. PostScript describes pages by using mathematical formulas (cubic splines, line segments, etc.) that represent shapes rather than by specifying individual pixels in a bit-mapped graphic image. PostScript encodes type faces into outlines that can be reconstructed at the proper size and than filled in to solidify the outline. This unique system of type face definition is used to generate fonts of virtually any size through spline interpolation, and is designed in PostScript for a wide variety of font styles.

For multilevel images a number of algorithms for scaling have been investigated (e.g., [6]–[8]). These algorithms are based on interpolation techniques, and they are aimed at increasing or decreasing the dimensionality of the whole image rather than a particular object. These algorithms do not readily lend themselves to scaling of binary images, since the scaled image will not necessarily remain binary.

Our investigation is to develop a character scaling algorithm based totally on the contours of the character (see Fig. 1) for the purpose of scaling camera captured fonts. Thus, border detection is needed in this work, and a mapping transformation will be developed.

## II. Algorithm

A general block diagram of the various steps in the algorithm is shown in Fig. 1. The steps required to scale a character are as follow.